Metal Hexaammine as a Bulky Cation: Structural and Property Studies of $[M(NH_3)_6]Cu_8Sb_3S_{13}$ (M = Mn, Fe, Ni) and $[Fe(NH_3)_6]AgES_4$ (E = As, Sb)

George L. Schimek and Joseph W. Kolis*

Department of Chemistry, Clemson University, Clemson, South Carolina 29634-1905

Gary J. Long

Department of Chemistry, University of Missouri−Rolla, Rolla, Missouri 65401-0249

Received February 17, 1997. Revised Manuscript Received August 18, 1997[⊗]

Five new compounds, which bring together two classical groups, Werner transition-metal hexaammine complexes and sulfosalts, have been prepared from supercritical ammonia. They form in two different structure types which are built from traditional octahedrally coordinated transition-metal hexaammine cations and anionic networks that can be described as metalated derivatives of sulfosalts. The anionic framework of compound **I**, $[Fe(NH_3)_6]Cu_8Sb_3S_{13}$, is built around a central Cu_8S_{13} core in which copper atoms are surrounded by sulfur atoms in a very distorted tetrahedral coordination. These copper sulfide cores are linked together through bridging antimony atoms which assume a very regular tetrahedral coordination of sulfur atoms. The three mutually orthogonal channels created by the anion are filled with $Fe(NH_3)_6$ cations. In $[Fe(NH_3)_6]AgES_4$ (E = Sb or As), **II** and **III**, respectively, the anionic framework is a one-dimensional chain built from alternating E− and Ag−sulfide tetrahedra that share opposite edges. In this structure type, hydrogen bonding apparently plays a role in the packing of the $Fe(NH_3)_6$ cations and anionic chains. Substitution of Fe with Mn or Ni in the synthesis results in compounds with the structure type observed in **I**. The synthetic routes and characterization, via X-ray crystallography, Mössbauer and IR spectroscopies, DSC, TGA, and bond valence sums are described. Crystal data: **I**, black cube, $F\bar{4}3c$, $a = 17.800(2)$ Å, $V = 5640(1)$ Å^3, $Z = 8$, R (wR) = 0.0432 (0.0472); **II**, yellow parallelepiped, $P\bar{4}n2$, $a = 10.274(2)$ Å, $c = 6.707(2)$ Å, $V = 707.9(3)$ Å^3, $Z = 2$, R (wR) = 0.0249 (0.0297); **III**, yellow polyhedron, $P\bar{4}n2$, $a = 10.244(2)$ Å, $c = 6.660(2)$ Å, $V = 698.8(3)$ Å^3, $Z = 2$, R (wR) = 0.0372(0.0423).

Introduction

An excellent technique for the custom design of open-framework materials involves the self-assembly of framework building blocks around a template, which is specifically selected to create a pore. If this template can subsequently be removed without disruption of the framework, a microporous solid with custom-designed voids can be obtained. This strategy has worked with great success in oxide-based frameworks such as zeolites.[1] Recently this approach has also been used with some degree of success in sulfide-based frameworks as well.[2] In this case the approach is more complicated because the template is usually removed by oxidation at slightly higher temperatures, and care must be taken that the sulfide framework is not oxidized as well.

In our laboratory we have been able to demonstrate that supercritical amines are excellent solvents for the spontaneous self-assembly of many sulfide-based frameworks with varying degrees of complexity.[3] In general, we have found that alkali metal chalcogenide-based polynuclear anions react readily with coinage metals to form a variety of ternary and quaternary solids containing an alkali metal, a monovalent transition metal, and in most cases, unique main-group building blocks. For example,

$$K_2S_4 + 6Ag \rightarrow K_2Ag_6S_4{}^4$$

$$2\text{“}CsSbS_2\text{”} + 3Ag + 3S \rightarrow Cs_2Ag_3Sb_3S_7{}^5 \qquad (1)$$

The metal sulfide frameworks often appear to be self-supporting in nature and are typically low-dimensional solids, which are a result of the presence of the alkali-metal cations in the lattice. The low-dimensional nature of the solids, their open, self-supporting appearance, and the sensitivity of the structure based on the identity of the cation strongly suggest that the use of larger cations as templates should lead to more open frameworks with large potential voids.

We have been systematically investigating the replacement of monovalent alkali metal cations with di-

* Fax: 864-656-6613. E-mail: KJOSEPH@Clemson.edu.

[⊗] Abstract published in *Advance ACS Abstracts,* October 1, 1997.

(1) Davis, M. E.; Lobo, R. F. *Chem. Mater.* **1992**, *4*, 756 and references therein.

(2) (a) Bowes, C. L.; Ozin, G. A. *Adv. Mater.* **1996**, *8*, 13 and references therein. (b) Tan, K.; Parise, J. B.; Darovsky, A. *Chem. Mater.* **1996**, *8*, 448 and references therein. (c) Parise, J. B. *Science* **1991**, *251*, 293.

(3) (a) Schimek, G. L.; Pennington, W. T.; Wood, P. T.; Kolis, J. W. *J. Solid State Chem.* **1996**, *123*, 277. (b) Wood, P. T.; Schimek, G. L.; Kolis, J. W. *Chem. Mater.* **1996**, *8*, 721. (c) Jerome, J. E.; Wood, P. T.; Pennington, W. T.; Kolis, J. W. *Inorg. Chem.* **1994**, *33*, 3, 1733. (d) Wood, P. T.; Pennington, W. T.; Kolis, J. W. *Inorg. Chem.* **1994**, *33*, 1556.

S0897-4756(97)00095-1 CCC: $14.00

and trivalent metal cations in an attempt to generate new structure types with more interesting magnetic and electronic properties. However, performing these reactions in supercritical ammonia in the presence of di- and trivalent transition-metal cations results in ammonia coordinating to the metal center, sequestering the metal and forming a large cationic species. We have isolated a variety of complex sulfide-based frameworks containing Werner type metal coordination complexes as countercation templates.[6] Also, in the presence of trivalent lanthanide cations, a number of silver and copper polysulfides can be isolated which contain the first homoleptic lanthanide ammine complexes as countercations (eq 2).[7]

$$\mathrm{Ln + M + S_8 \rightarrow NH_3 \rightarrow [Ln(NH_3)_{\mathit{x}}][M(S_4)_2]}$$
$$(\mathrm{Ln = La, Yb;\ M = Cu, Ag;}\ x = 8, 9) \quad (2)$$

It should be noted that Li and co-workers also isolated a number of interesting chalcogenide-based compounds containing metal coordination complexes from superheated ethylenediamine (en).[8] In this case, the larger size of the coordinating en ligand leads to a much larger cationic complex. As a result, the templating effect does not effectively create a pore but results more commonly in one-dimensional chains or discrete molecular species.

We are especially attracted to supercritical ammonia as a solvent, because its volatility may make it easier to remove under relatively mild conditions, creating voids that contain catalytically active metal and leaving the framework intact. In this paper we report several unusual solids based on metal antimony sulfide frameworks wherein iron hexaammine acts as a template entrapped in voids within the lattice. Crystal structures of these compounds, along with more complete electronic characterization and thermal decomposition investigations are presented.

Experimental Procedure

IR spectra were taken as Fluorolube or Nujol mulls between polyethylene sheets on either a Nicolet Magna-IR 550 or Nicolet 20F/5DX spectrometer.

Synthesis $[Fe(NH_3)_6]Cu_8Sb_3S_{13}$ (I). The title phase can be synthesized using methods similar to those first reported by Rabenau.[9] Stoichiometric quantities (16:128:24:17 mole ratio) of Fe (Matheson Coleman & Bell, >98%), Cu (Strem, 99.9%), Sb_2S_3 (Strem, 98%), and S_8 (Mallinckrodt, 99.9%) on a 160 mg scale were loaded into fused silica tubes (5 mm i.d., 7 mm o.d., 1.2 cm^3 sealed volume) under an argon atmosphere in a Vacuum Atmospheres drybox. The tubes were subsequently evacuated ($\sim 10^{-3}$ Torr), and approximately 0.5 mL (40% fill) of NH_3 was distilled onto the reagents. The tubes were flame-sealed after freezing the solvent and then thawed to give dark red solutions and some insoluble reagents. The fused silica tubes were loaded into a high-pressure autoclave, and an argon counter-pressure of 3500 psi was applied. The apparatus was heated at 160 °C for 4 days. After cooling, the liquid NH_3 was colorless. In the molar ratio given above, the product is heavily contaminated with Cu_3SbS_4. It was determined that a 2−3-fold molar excess of iron metal promoted maximum yield of **I**. IR (cm^{-1}): 3370(w), 1635(m), 1244(m), 635(br), 555(br), 365(m), 283(m). With this improved synthetic route, the title compound is formed as a black microcrystalline powder that is still partially contaminated with Cu_3SbS_4 and three unindexable *d* spacings with relative intensities of 4% or less (Figure 1). It is thought that these minor peaks belong to a new phase that we cannot identify. The fate of the excess Fe is not known, but it is probably still in solution (vide infra). Growth of black cubes of **I** large enough for single-crystal X-ray diffraction studies was promoted by the presence of alkali metal carbonate.

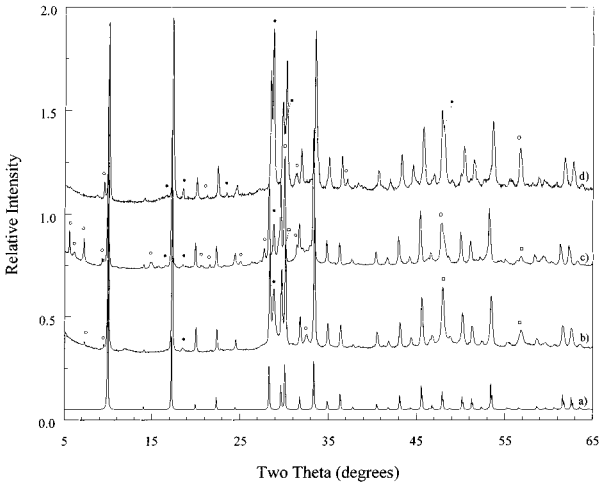

Figure 1. X-ray powder diffraction patterns of (a) $[Fe(NH_3)_6]Cu_8Sb_3S_{13}$ calculated from single-crystal data, (b) $[Fe(NH_3)_6]Cu_8Sb_3S_{13}$ as synthesized, (c) $[Mn(NH_3)_x]Cu_8Sb_3S_{13}$ as synthesized, and (d) $[Ni(NH_3)_x]Cu_8Sb_3S_{13}$ as synthesized. Denoted peaks: filled circles are famatinite, open squares are peaks due to the title phase and famatinite overlapping, and open circles are unknown.

Synthesis $[M(NH_3)_x]Cu_8Sb_3S_{13}$ (M = Mn, Ni). A 2−3-fold molar excess of $MnCO_3$ was loaded with stoichiometric quantities of $128Cu{:}24Sb_2S_3{:}17S_8$ on a 150 mg scale and reacted at identical conditions as used for **I**. A black microcrystalline powder of $[Mn(NH_3)_x]Cu_8Sb_3S_{13}$ was obtained. IR (cm^{-1}): 1230(m), 621(br), 540(sh), 366(s), 282(w). Minor impurities were attributed to Cu_3SbS_4 and a trace compound with 10 unassigned peaks with relative intensities less than 25% (Figure 1). If a 2-fold molar excess of Ni metal is utilized in place of $MnCO_3$, with the same ratio and on the same scale of the other reagents, and reaction conditions as given above, the $[Ni(NH_3)_x]Cu_8Sb_3S_{13}$ phase is formed. IR (cm^{-1}): 3367(w), 1258(m), 956(br), 634(w), 598(br), 366(s), 350(sh), 284(m). Again, this phase forms with Cu_3SbS_4 as one impurity and four extraneous peaks with relative intensities less than 8% (Figure 1). We attribute the minor impurities to the trace presence of a new unidentifiable phase. Both of the Mn and Ni phases are black, microcrystalline powders and could be indexed from their respective XRD patterns based on the structural information of **I**.

Synthesis $[Fe(NH_3)_6]AgES_4$, II (E = Sb) and III (E = As). Compounds **II** and **III** were synthesized in minimal yield from stoichiometric quantities (16:16:8:5 mole ratio) of Fe, Ag, M_2S_3 (when M = As: Johnson-Matthey, 99.9%) and S_8 on a 150 mg scale. Reagents were loaded as above and gave intense red-purple ammonia solutions. The tubes were subsequently loaded into an autoclave as above and heated at 160 °C for 4.5 days. After heating, both systems had light yellow ammonia solutions. A few yellow parallelepipeds of **II** formed with the bulk material which was predominantly Ag_3SbS_3, $AgSbS_2$ and FeS_2. For **III**, a few yellow and orange polyhedra were intermixed with the bulk yellow and black powder. The yellow and orange crystals were determined to be the title

(4) Wood, P. T.; Pennington, W. T.; Kolis, J. W. *J. Chem. Soc., Chem. Commun.* **1993**, 235.
(5) Jerome, J. E.; Schimek, G. L.; Pennington, W. T.; Kolis, J. W., to be submitted.
(6) Young, D. M.; Schimek, G. L.; Wilcenski, S. M.; Kolis, J. W. *Inorg. Chem.*, submitted.
(7) Young, D. M.; Schimek, G. L.; Kolis, J. W. *Inorg. Chem.* **1996**, *35*, 7620.
(8) (a) Li, J.; Rafferty, B. G.; Mulley, S.; Proserpio, D. M. *Inorg. Chem.* **1995**, *34*, 6417. (b) Li, J.; Chen, Z.; Emge, T. J.; Proserpio, D. M. *Inorg. Chem.* **1997**, *36*, 1437.
(9) Rabenau, A. *Angew. Chem., Int. Ed. Engl.* **1985**, *24*, 1026.

phase and $(NH_4)Ag_2AsS_4$,[10] respectively, while the bulk was found to be $AgAsS_2$ and FeS_2. For samples that appeared to contain a higher quantity of **III**, exposure to the atmosphere caused the sample to turn black and gave a weakly crystalline XRD pattern. No significantly improved synthetic route to **II** or **III** was found.

Similar reactions utilizing various metal powders (Mn,Fe,-Ni), $MnCO_3$, $Fe_3(CO)_{12}$, Fe_2O_3, and $FeCl_2$ with the above stoichiometries and temperature conditions were also loaded with varying amounts of ammonium carbonate, with the intention of promoting crystallization and/or yield. However, these attempts to grow larger crystals did not work. Other transition metals that are known to form hexaammine cations were also explored with the Cu/Sb/S system, in particular, chromium (as $Cr(CO)_6$ or Cr), cobalt (as $CoCO_3 \cdot xH_2O$) and ruthenium (as $Ru_3(CO)_{12}$). The major product identified in all these cases was Cu_3SbS_4.

X-ray Crystallography. *Powder diffraction*: Phase purity of microcrystalline samples was analyzed at room temperature with a Scintag XDS 2000 $\theta-\theta$ diffractometer equipped with Cu Kα radiation ($\lambda = 1.540\,562$ Å).

Single-crystal diffraction: Single crystals of the title phases (**I**−**III**) were isolated under Nujol after decanting and freezing out the ammonia solution. They were subsequently mounted in glass capillaries with quick-drying epoxy. A Rigaku AFC7R four-circle diffractometer equipped with graphite-monochromated Mo Kα radiation ($\lambda = 0.710\,73$ Å) was utilized. Lattice parameters were derived from at least 22 randomly located and centered reflections with a 2θ range of 12.8−34.5°. Three standard reflections were measured every 100 reflections and showed negligible variation in intensity throughout the data collection for **I** and **II**; however, decay of ~19% was measured for **III**. An $\omega-2\theta$ scan mode (4°/min for **I** and 8°/min for **II** and **III**, with ≤3 rescans) was used and data were collected from $3 < 2\theta < 55°$, $4 < 2\theta < 60°$ and $3 < 2\theta < 50°$ for **I**−**III**, respectively, in the *hkl* octant. Data were collected at room temperature for **I** and **III** and at −100 °C for **II**. The number of reflections measured was 1783, 1237, and 1052, of which 306, 947, and 622 were unique and 145, 504, and 220 were observed with $F > (5, 6 \text{ and } 4)\sigma(F)$ for **I**, **II**, and **III**, respectively. The linear absorption coefficient with Mo Kα radiation was 10.185, 4.832, and 5.359 mm^{-1} for **I**−**III**, respectively. The intensity data were corrected for Lorentz and polarization effects.

For **I**, the noncentrosymmetric space group $F\bar{4}3c$ was chosen based upon the centering condition and the systematic absences $0kl$: $k, l = 2n + 1$; hhl: $h, l = 2n + 1$ and $00l$: $l = 2n + 1$. These systematic absences also correspond to the space group $Fm\bar{3}c$. However, the solution obtained in the noncentrosymmetric space group gave a chemically reasonable structure, while the refinement in the centrosymmetric space group did not. Finally, in $F\bar{4}3c$, the reported positions of the sulfur atoms do not allow the presence of mirror planes perpendicular to the primary axes, as required by $Fm\bar{3}c$, and therefore the choice of the noncentrosymmetric space group $F\bar{4}3c$ was confirmed. As justification of the centered cell, the *hkl* data with $h, k, l = 2n + 1$ were extraordinarily weak. If they are considered unobserved, only $h, k, l = 2n$ are observed and one must consider a primitive cubic subcell with cell lengths one-half of those reported for $F\bar{4}3c$. The structural models obtained from this smaller cell gave unreasonable bond distances between sulfur atoms.

The space group chosen for **II** and **III** was $P\bar{4}n2$, based upon the systematic absences $0kl$: $k + l = 2n + 1$; $0k0$: $k = 2n + 1$ and $00l$: $l = 2n + 1$. Two other space groups, $P4_2nm$ and $P4_2/mnm$, also have these same systematic absences. On the basis of a superior refinement in $P\bar{4}n2$, it was determined that the face diagonal mirror planes required in the two alternative space group choices could not be present, thus eliminating both options.

The structures were solved by direct methods in the space groups discussed above, and refined on $|F|$ by full-matrix, least-squares techniques with a combination of teXsan and SHELX-TL-Plus software.[11] Scattering factors for all atoms were taken from the source programs utilized. An empirical (three ψ scans) absorption correction (transmission range 0.91−1.00) was utilized in the case of **I**; for **II** a DIFABS[12] correction (0.714−1.181) was applied to the calculated intensity data for the refinement in which all atomic thermal parameters were refined isotropically, and in **III** no correction was applied. A decay correction for **III** showed no significant improvement and therefore was not used. All non-hydrogen atom thermal parameters were refined anisotropically. Hydrogen atoms on the amine nitrogens in **I** were not located or generated, due to the positional disorder that would be necessitated from the local site symmetry. However, in **II**, the hydrogen atoms on N1 were positionally refined with isotropic thermal parameters. The hydrogen atoms on N2 of **II** were located from a difference map, set at $^1/_2$ occupancy (due to site symmetry requirements), and positionally and thermally fixed. In the case of **III**, a few hydrogen atoms were located from difference maps and then utilized to generate the remaining hydrogen atoms with ideal geometry (109.5°) and bond distances (d(N−H) = 0.9 Å). All amine hydrogens in **III** were then fixed positionally and refined with a group hydrogen isotropic thermal parameter.

A noteworthy feature of the isotropic temperature factors of the atoms in **I**, $[Fe(NH_3)_6]Cu_8Sb_3S_{13}$, is that U_{eq} for S2 is about 10 times larger than that of S1. The S2 atom is too small, relative to the size of the cavity in which it resides (vide infra). Two other possibilities were considered, but these were discounted or not crystallographically possible in $F\bar{4}3c$. Either a lighter atom resides in the cavity or the atom is disordered. In the former case, refinements were undertaken to replace S2 with a lighter atom, in particular oxygen. However these refinements resulted in a nonpositive definite isotropic temperature factor for that atom. The second possibility, a disordered S2 is more likely the case. Refinements in which S2 was taken off the intersection of the 2- and 3-fold rotation axes were ill-behaved. This is because suitable positioning of S2 to create reasonable Cu−S bond distances cannot be crystallographically achieved. For example, movement off the 2-fold rotation axis generates 3 times as many positions as needed, all of which are not geometrically reasonable with respect to the outer copper sulfide network. Similar circumstances occur with movement off the 3-fold rotation axis or placement of the atom on a general position. It is our contention that S2 is statistically distributed over many positions, any one of which satisfies only a few of the copper coordination spheres. Thus the rather large thermal motion is symptomatic of the placement of the S2 atom in its average, but not actual, position. The rather large anisotropic motion of Cu2 also may be indicating that it is attempting to compensate for the overly long Cu−S bond distances. This would also cause the copper atom to deviate even further from trigonal planar geometry toward tetrahedral coordination.

Crystallographic details are given in Table 1. Residual values for the correct absolute structures and incorrect enantiomorphs are listed in the table, since all three compounds are noncentrosymmetric. Compounds **II** and **III** are isomorphous; however, the refinement models with the lower residuals for these two phases have opposite handedness. Positional and isotropic thermal parameters are listed in Table 2.

Mössbauer Spectroscopy. The Mössbauer spectra were measured on a conventional constant-acceleration spectrometer which utilized a room-temperature rhodium matrix cobalt-57 source and was calibrated at room temperature with natural α-iron foil. The resulting spectra were fit with two symmetric Lorentzian quadrupole doublets by using standard computer minimization programs.

Stability Studies. *Differential scanning calorimetry and thermogravimetric analysis*: The thermal stabilities of the

(10) Auernhammer, M.; Effenberger, H.; Irran, E.; Pertlik, F.; Rosenstingl, J. *J. Solid State Chem.* **1993**, *106*, 421.

(11) (a) teXsan: Single Crystal Structure Analysis Software, Version 1.6b, 1993. Molecular Structure Corp., The Woodlands, TX 77381. (b) SHELXTL-Plus: Sheldrick, G. M. Siemens Analytical X-ray Instruments, Inc., Madison, WI 53719.

(12) Walker, N.; Stuart, D. *Acta Crystallogr.* **1983**, *A39*, 158.

Table 1. X-ray Crystallographic Data[a]

formula	$[Fe(NH_3)_6]Cu_8Sb_3S_{13}$	$[Fe(NH_3)_6]AgSbS_4$	$[Fe(NH_3)_6]AgAsS_4$
formula wt	1448.4	515.9	469.1
crystal system	cubic	tetragonal	tetragonal
space group (No.), Z	$F\bar{4}3c$ (219), 8	$P\bar{4}n2$ (118), 2	$P\bar{4}n2$ (118), 2
a (Å)	17.800(2)	10.274(2)	10.244(2)
c (Å)		6.707(2)	6.660(2)
vol (Å^3)	5640(1)	707.9(3)	698.8(3)
calcd density (g/cm^3)	3.41	2.42	2.23
crystal dimensions (mm)	0.05 × 0.05 × 0.05	0.10 × 0.08 × 0.15	0.10 × 0.10 × 0.10
2θ range (deg), octants	3−55, h,k,l	4−60, h,k,l	3−50, h,k,l
refl collected (unique)	1783 (306)	1237 (947)	1052 (622)
obsd, $F > X\sigma(F)$, R_{int}	145, 5.0, 0.0407	504, 6.0, 0.0369	220, 4.0, 0.0364
variables	25	44	32
μ, mm^{-1}	10.185	4.832	5.359
transmission range	0.91−1.00	0.714−1.181	na
secondary extinction (×10^{-7})	na	2.93	na
R^b, R(enant)^c	0.0432, 0.0449	0.0249, 0.0259	0.0372, 0.0482
wR^d, wR(enant)^c	0.0472, 0.0478	0.0297, 0.0301	0.0423, 0.0576
S^e, S(enant)^c	1.45, 1.46	1.75, 1.77	1.09, 1.50
residual (e$^-$/Å^3), max shift	2.90/−2.04, 0.008	1.52/−1.55, 0.0009	1.01/−0.64, 0.0005

[a] All data were collected at 295 K for **I** and **III** and 173 K for **II**, Mo Kα radiation, $\lambda = 0.7107$ Å. Decay was <±2% for **I** and **II** and ~19% for **III**. [b] $R = \sum||F_o| - |F_c||/\sum|F_o|$. [c] Residuals observed for the model compounds with the incorrect absolute structure. [d] $wR = [\sum w\{|F_o| - |F_c|\}^2/\sum w|F_o|^2]^{1/2}$; $w = 1/\sigma^2\{|F_o|\}$. [e] $S = [\sum(|F_o|_i - |F_c|_i)/\sigma_i]/(n - m)$; $i = 1$ to n.

Table 2. Atomic Coordinates and Equivalent Isotropic Thermal Parameters (Å^2)

atom	Wyckoff	X	Y	Z	U_{eq}[a]
		$[Fe(NH_3)_6]Cu_8Sb_3S_{13}$			
Sb	24c	3/4	3/4	0	0.0160(7)
Cu1	32e	0.8365(4)	0.8365	0.8365	0.020(1)
Cu2	32e	0.6632(8)	0.6632	0.6632	0.072(3)
Fe	8a	0	0	0	0.030(2)
S1	96h	0.754(2)	0.8602(4)	0.9271(4)	0.018(2)
S2	8b	3/4	3/4	3/4	0.14(1)
N	48f	0.876(1)	0	0	0.04(2)
		$[Fe(NH_3)_6]AgSbS_4$			
Sb	2a	0	0	0	0.0120(2)
Ag	2b	0	0	1/2	0.0324(3)
Fe	2c	0	1/2	1/4	0.0194(4)
S	8i	−0.1593(1)	0.0824(1)	0.2146(2)	0.0166(5)
N1	8i	0.1014(6)	0.6138(5)	0.4799(9)	0.023(2)
N2	4g	−0.1555(4)	0.6555	1/4	0.030(3)
		$[Fe(NH_3)_6]AgAsS_4$			
As	2a	0	0	0	0.032(2)
Ag	2b	0	0	1/2	0.059(2)
Fe	2d	0	1/2	3/4	0.033(1)
S	8i	−0.0769(5)	−0.1504(5)	0.1986(7)	0.033(2)
N1	8i	−0.101(2)	0.382(2)	0.521(2)	0.048(8)
N2	4g	0.157(1)	0.343	3/4	0.047(6)

[a] The equivalent isotropic temperature factor, U_{eq}, is defined as $^1/_3\{\sum_i\sum_j(U_{ij}a^*_ia^*_j\bar{a}_i\cdot\bar{a}_j)\}$ where the summations of i and j range from 1 to 3.

prepared title phases were examined with a TA Instruments Thermal Analyst 2000 equipped with a 910 differential scanning calorimeter (DSC) or a TA Instruments Thermal Analyst 3100 equipped with a 951 thermogravimetric analyzer (TGA). For DSC, ~15 mg samples were loaded into aluminum pans and hermetically sealed in an argon-filled drybox. These samples were referenced against a blank aluminum pan and heated from 30 to 500 °C at 10 °C/min under a helium gas purge. For TGA, the 15−30 mg samples were loaded into an open quartz boat, placed on the balance, and the system closed and purged with nitrogen gas for 3 h before ramping at 10 °C/min from room temperature to 600 °C.

Reaction chemistry: Samples of pure famatinite, Cu_3SbS_4, were subjected to the same DSC conditions as above and appear to be reactively inert, with the exception of an endothermic transition at ~320 °C. The residual famatinite present in all samples thus acted as an internal standard for the DSC studies and subsequent XRD work performed. Because experimental DSC investigations utilize only small quantities of sample, heat treatments on larger amounts of the Mn- and Ni-substituted phases of **I** were performed to make XRD characterization more convenient. In these cases, approximately 50−100 mg of each compound was loaded into quartz tubes, evacuated, sealed, and then heated with a furnace for approximately 1 day. The setpoint temperatures were derived from DSC results. For **I** with M = Mn, the temperatures were 275 and 500 °C, and with M = Ni, the temperatures were 250 and 500 °C.

Three experiments were performed to indicate that ammonia was not readily removed from the lattice of **I** when M = Fe. (1) A 50 mg sample of microcrystalline **I** was loaded into a round-bottom flask and subjected to dynamic vacuum for 3 weeks at room temperature. On the basis of powder diffraction, the lattice was still intact. (2) A 50 mg sample of microcrystalline **I** was loaded into a vial and soaked in 5 mL of water for 3 weeks. Afterward, no pH change of the water was observed based upon a litmus paper test. (3) DSC and TGA studies show the loss of ammonia *only* with a concurrent decomposition of the anionic framework (vide infra).

Structural Description

The three-dimensional anionic network found in $[Fe(NH_3)_6]Cu_8Sb_3S_{13}$, consisting of copper sulfide cores linked together by antimony centers, forms channels in which the iron hexaammine cations reside (Figure 2). The fundamental anionic unit is found in each of the eight octants of the unit cell. The connectivity within this fragment, $Cu_8Sb_6S_{25}$, is more easily understood when visualized parallel to the 3-fold rotation axis (Figure 3). It is built from eight CuS_4 tetrahedra sharing a common sulfur vertex (S2, located at the intersection of the 2- and 3-fold rotation axes). This close proximity of eight tetrahedra necessitates that these polyhedra also share S1 to S2 edges. All S1 atoms are shared among two Cu and one Sb atoms. The antimony atoms bridge across the outer vertexes of the Cu_8S_{13} core. The sulfur atoms (S1) surrounding each antimony atom reside on general positions and serve to link neighboring Cu_8S_{13} cores. The alternating bridging pattern of the SbS_4 tetrahedra, as viewed parallel to any of the cell axes, does not allow the necessary translational symmetry for a primitive cubic unit cell with 1/8 the volume (Figure 2).

The coordination environments of the antimony and copper atoms bear some important details. Antimony atoms reside on a $\bar{4}$ symmetry site, and thus the bridging SbS_4 tetrahedra have quite regular coordination and bonding (averaging 2.353(7) Å and 110(3)°),

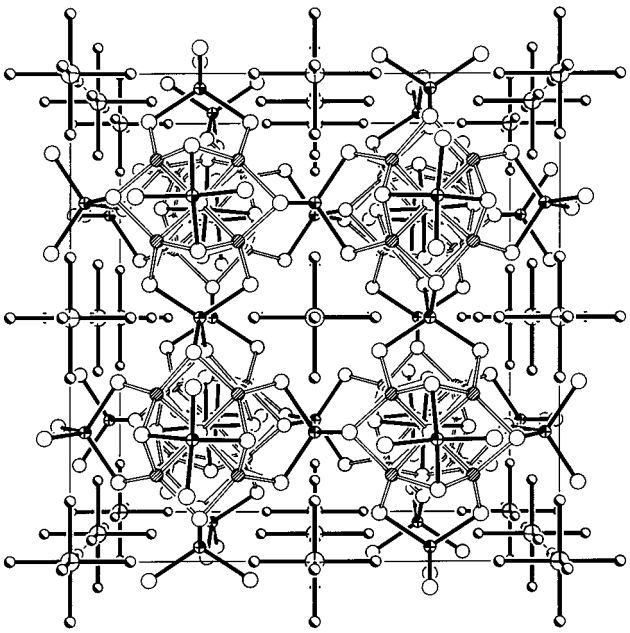

Figure 2. Unit-cell view of $[Fe(NH_3)_6]Cu_8Sb_3S_{13}$, **I**. Atom types: antimony atoms 70% full thermal ellipsoids, iron atoms 70% principal ellipsoids, copper atoms striped spheres, sulfur atoms open spheres, and nitrogen atoms highlighted spheres. Copper−sulfur bonds open.

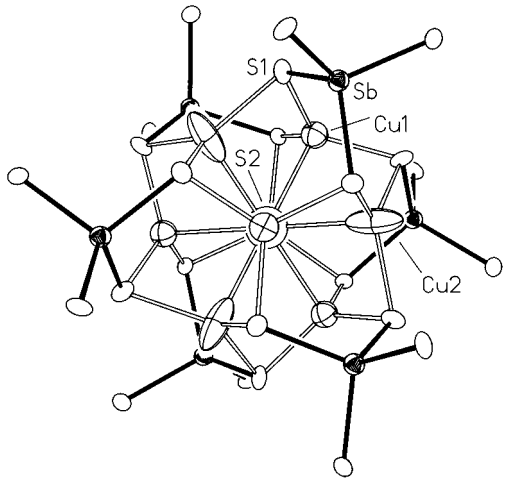

Figure 3. Fragment of the metallosulfide cluster, $Cu_8Sb_6S_{25}$, found in **I**. Atom types: antimony atoms full thermal ellipsoids, copper atoms principal ellipsoids and sulfur atoms boundary ellipsoids, all at the 70% probability level. Copper−sulfur bonds open.

typical nonmolecular antimony sulfide tetrahedra have bond distances and angles that range from 2.33 to 2.36 Å and 104−114°, respectively, as found in MAg_2SbS_4 and M_2AgSbS_4 (M = K and Rb).[3a] In contrast, the copper sulfide tetrahedra at the core of the anionic unit are very distorted. In fact, the anisotropic nature of the thermal parameters of Cu2 imply that it is not residing in a completely suitable coordination environment. This behavior could be expected when it is noted that the S2 atom is in a site far too large for its bonding radius and thus also exhibits large thermal motion. Both Cu atoms lie on 3-fold rotation axes. Cu−S1 bond distances average 2.27(7) Å, while Cu−S2 distances are 2.68(2) Å, a striking difference. Typical tetrahedral Cu−S bond distances range from 2.31 to 2.45 Å in KCu_4S_3,[13] 2.34 to 2.39 Å in $BaErCuS_3$,[14] and 2.18 to 2.45 Å in $KCuCe_2S_6$ and $K_2Cu_2CeS_4$.[15] The significant difference in bond distances could suggest that the copper coordination is more aptly described as trigonal pyramidal. The distances that Cu1 and Cu2 reside above their respective basal planes of S1 atoms are 0.21 and 0.35 Å. $Cu_{12}Sb_4S_{13}$[16] and $NH_4Cu_7S_4$[17] both contain a copper atom which is essentially three coordinate to sulfur atoms. The Cu−S bond distances in the former range from 2.31 to 2.37 Å and in the latter, 2.234 to 2.272 Å. These distances are more comparable to those determined in **I**.

The iron atoms are located on positions with 23 site symmetry: at the origin, face centers, body center, and halfway along each cell edge. Each iron center has a full complement of six ammonia ligands with crystallographically imposed octahedral coordination. Nitrogen atoms are located along the 2-fold rotation axes parallel to the primary axes with Fe−N bond distances of 2.21(3) Å. Until recently, surprisingly few iron hexaammines had been structurally characterized, since many simple halide salts of the $Fe(NH_3)_6$ cations are related to the fluorite-like K_2PtCl_6 structure type. These phases were initially studied when crystallography was in its infancy, and nitrogen atoms were generally not located.[18] However, the recent crystallographic reexamination of $M(NH_3)_6X_2$ (M = V, Cr, Mn, Fe, Co, or Ni; X = Cl, Br, or I) has revealed Fe−N bond distances of 2.206(8), 2.215(3), and 2.229(5) Å for X = Cl, Br, and I, well within the distance observed for **I**.[19] A complete listing of bond distances is given in Table 3.

Hydrogen bonding, N−H···S, between the cation and anion in **I** cannot be conclusively demonstrated. However, if hydrogen atoms are generated with ideal geometry (0.9 Å, 109.5°) the shortest hydrogen atom to S1 atom interaction is approximately 2.76 Å, well within the van der Waals radii of 3.05 Å.[20]

Compounds **II** and **III** are isostructural and contain a far less complicated atomic arrangement than that observed in **I**. Both structures are composed of isolated one-dimensional anionic chains and iron hexaammine cations (Figure 4). The anionic chain is built from $(ES_4)^{3-}$ tetrahedra (E = Sb or As) in which two opposite edges are linked by Ag(I), creating edge-shared, alternating E and Ag tetrahedra. Again, the pnictide tetrahedra have very regular tetrahedral geometry while the silver cations accommodate a very distorted tetrahedral geometry in order to tie neighboring $(ES_4)^{3-}$ units together. The E and Ag atoms reside on two different $\bar{4}$ symmetry sites. Bond angles around E range from 104.03(7) to 112.26(4)° and E−S bond

(13) Brown, D. B.; Zubieta, J. A.; Vella, P. A.; Wrobleski, J. T.; Watt, T.; Hatfield, W. E.; Day, P. *Inorg. Chem.* **1980**, *19*, 1945.
(14) Wu, P.; Christuk, A. E.; Ibers, J. A. *J. Solid State Chem.* **1994**, *110*, 337.
(15) Sutorik, A. C.; Albritton-Thomas, J.; Kannewurf, C. R.; Kanatzidis, M. G. *J. Am. Chem. Soc.* **1994**, *116*, 7706.
(16) Wuensch, B. J. *Z. Kristallogr.* **1964**, *119*, 437 and references therein.
(17) Gattow, Von G. *Acta Crystallogr.* **1957**, *10*, 549.
(18) (a) Wyckoff, R. W. G. In *Crystal Structures*, 2nd ed.; Interscience Publishers: New York, 1965; Vol. 3, p 873. (b) Olovsson, I. *Acta Crystallogr.* **1965**, *18*, 889.
(19) (a) Essmann, R.; Kreiner, G.; Niemann, A.; Rechenbach, D.; Schmieding, A.; Sichla, T.; Zachwiega, U.; Jacobs, H. *Z. Anorg. Allg. Chem.* **1996**, *622*, 1161. (b) Jacobs, H.; Bock, J.; Stüve, C. *J. Less-Common Met.* **1987**, *134*, 207.
(20) Pauling, L. *The Nature of the Chemical Bond*, 3rd ed.; Cornell University Press: Ithaca, NY, 1960.

Table 3. Bond Distances (Å) and Angles (deg)

	$[Fe(NH_3)_6]Cu_8Sb_3S_{13}$		
Sb−S1	2.353(7) × 4	S1−Sb−S1[d]	113.1(3) × 2
Cu1−S1	2.33(2) × 3	S1−Sb−S1[e]	107.7(2) × 4
Cu1−S2	2.67(1)	N1−Fe−N1[f]	180.0(1) × 3
Cu2−S1[a]	2.21(2) × 3	N1−Fe−N1[b]	90.0(1) × 12
Cu2−S2	2.68(2)	Sb−S1−Cu1	101.9(7)
Fe−N	2.21(3) × 6	Sb−S1−Cu2[a]	105.5(6)
S1−Cu1−S1[b]	119.0(2) × 3	Cu1−S1−Cu2[a]	85.6(7)
S1−Cu1−S2	95.8(6) × 3	Cu2−S2−Cu2[d]	109.5(1) × 6
S1[a]-Cu2−S1[c]	117.9(4) × 3	Cu1−S2−Cu2	180.0(1) × 4
S1[a]-Cu2−S2	98.5(8) × 3	Cu2−S2−Cu1[d]	70.5(1) × 12
	$[Fe(NH_3)_6]AgSbS_4$		
Sb−S	2.338(1) × 4	N1−Fe−N1[i]	89.3(3) × 2
Ag−S	2.657(1) × 4	N1−Fe−N1[j]	90.9(3) × 2
Fe−N1	2.197(5) × 4	N1−Fe−N1[k]	175.3(3) × 2
Fe−N2	2.260(7) × 2	N1−Fe−N2	87.7(2) × 4
S−Sb−S[f]	104.03(7) × 2	N1−Fe−N2[j]	92.3(2) × 4
S−Sb−S[g]	112.26(4) × 4	N2−Fe−N2[j]	180.0(1)
S−Ag−S[f]	87.82(6) × 2	Sb−S−Ag	84.07(4)
S−Ag−S[h]	121.26(3) × 4		
	$[Fe(NH_3)_6]AgAsS_4$		
As−S	2.178(5) × 4	N1−Fe−N1[l]	87.9(9) × 2
Ag−S	2.651(5) × 4	N1−Fe−N1[j]	92.4(9) × 2
Fe−N1	2.21(2) × 4	N1−Fe−N1[m]	173.(1) × 2
Fe−N2	2.267(1) × 2	N1−Fe−N2	86.6(6) × 4
S−As−S[f]	105.2(3) × 2	N1−Fe−N2[j]	93.4(6) × 4
S−As−S[g]	111.6(1) × 4	N2−Fe−N2[j]	180.0(1)
S−Ag−S[f]	81.5(2) × 2	As−S−Ag	86.6(2)
S−Ag−S[h]	125.0(1) × 4		

[a] $x, 0.5 - y, 0.5 - x$. [b] z, x, y. [c] $0.5 - z, x, 0.5 - y$. [d] $0.5 - x, 0.5 - y, z$. [e] $y, 0.5 - x, -z$. [f] $-x, -y, z$. [g] $y, -x, -z$. [h] $y, -x, 1 - z$. [i] $-0.5 + y, 0.5 + x, 0.5 - z$. [j] $-x, 1 - y, z$. [k] $0.5 - y, 0.5 - x, 0.5 - z$. [l] $-1.5 + y, 0.5 + x, 1.5 - z$. [m] $0.5 - y, 0.5 - x, 1.5 - z$.

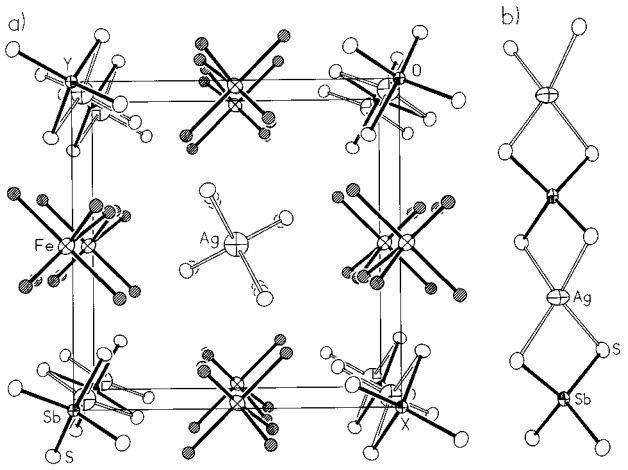

Figure 4. (a) Unit cell view of $[Fe(NH_3)_6]AgSbS_4$ parallel to the *c*-axis. (b) Anionic chain of trans edge-shared alternating metal tetrahedra. Atom types: antimony atoms full thermal ellipsoids, silver and iron atoms principal ellipsoids, sulfur atoms boundary ellipsoids (all at the 70% probability level) and nitrogen atoms striped spheres. Silver−sulfur bonds open and hydrogen atoms omitted for clarity.

distances of 2.338(1) and 2.178(5) Å for **II** and **III**, respectively, are comparable to other E(V)−S systems.[3,21] Long Ag−S bond distances (2.65 Å) and extremely distorted bond angles ranging from 81 to 125° in **II** and **III** have been observed previously in other compounds, for example, $RbAg_2SbS_4$ (2.48−2.78 Å, 90−148°), and in particular when silver atoms reside on $\bar{4}$ sites, such as those found in KAg_2SbS_4 (2.603 Å, 95.12° and 145.2°).[3a]

The iron center of **II** and **III** is positioned at the intersection of three mutually perpendicular 2-fold rotation axes and is not required to be strictly octahedrally coordinated by ammonia in $P\bar{4}n2$. However, the deviations from that geometry are only slight. Both **II** and **III** have four short (2.20 Å) and two slightly longer (2.26 Å) Fe−N bond distances. The former nitrogen atoms reside on general positions while the latter are situated on 2-fold rotation axes. Trans and cis bond angles within the iron hexaammine average 176(3)° and 90(3)°, respectively. Detailed bond distances and angles are given in Table 3.

In **II**, hydrogen atoms were located from difference maps and refined. There are five hydrogen-bonding interactions, ranging from 2.6(1) to 2.99(7) Å. These interactions would appear to be quite necessary in such a loosely packed structure type as that observed in **II** and **III**. The hydrogen bonding observed in **III** is similar to that in **II**; however, the quality of the data restricted any detailed analysis. More detailed information on the hydrogen bonding in **I**−**III** is included in the Supporting Information.

The $[Fe(NH_3)_6]AgES_4$ phases are essentially isomorphous with NH_4CuMoS_4.[22] In that compound, alternating Cu and Mo sulfide tetrahedra share opposite edges to generate the one-dimensional anionic chains that are separated by ammonium cations. The significant difference between the iron hexaammine compounds reported here (**II** and **III**) and the previously published phase is that the latter crystallizes in a body-centered unit cell. In **II** and **III**, the only atoms that violate the centering condition, and thus require a primitive unit cell, are the ammonia ligands.

Discussion

The reaction of iron powder with copper, antimony sulfide, and sulfur in supercritical ammonia leads to the formation of **I**. We originally thought that carbonate, from the starting reagent cesium carbonate, was a necessary component to generate a main-group anionic cluster. It is well-known that carbonate will induce disproportionation of antimony chalcogenides to polyanionic antimony chalcogenide chains in the temperature range we are investigating.[23] Indeed, these starting materials do lead to formation of the product, but the yield is low and other metal sulfosalts such as famatinite, Cu_3SbS_4, form in greater abundance. In the presence of excess iron powder without any carbonate present, the desired product forms in much greater yield as a microcrystalline powder. Using this altered synthetic route, the XRD pattern of this powder shows less intense diffraction from Cu_3SbS_4 with respect to **I**. Some inseparable amount of Cu_3SbS_4 always remains in every reaction. We found that the addition of cesium carbonate is necessary for the formation of well-crystallized single crystals of **I**, but we feel that the carbonate is acting as a mineralizer to promote crystal growth rather than as a reagent for compound formation. It is impossible to predict with any confidence a mechanism of such a complex reaction. However, iron is probably oxidized by sulfur to form iron sulfide, which can react

(21) Pertlik, F. *J. Solid State Chem.* **1994**, *12*, 170 and references therein.

(22) Binnie, W. P.; Redman, M. J.; Mallio, W. J. *Inorg. Chem.* **1970**, *9*, 1449.

(23) Sheldrick, W. S.; Kaub, J. *Z. Anorg. Allg. Chem.* **1986**, *535*, 179.

with stibnite to form antimony sulfide anions. For example, a possible balanced equation for this part of the reaction is

$$Fe + S \rightarrow FeS \quad (3a)$$

$$3FeS + Sb_2S_3 + 2S \rightarrow 3Fe^{2+} + 2SbS_4^{3-} \quad (3b)$$

The overall balanced equation is

$$16Fe + 128Cu + 24Sb_2S_3 + 17S_8 \rightarrow NH_3 \rightarrow 16[Fe(NH_3)_6]Cu_8Sb_3S_{13} \quad (3)$$

The oxidation of Fe in supercritical ammonia may be analogous to the base-induced reduction of sulfur by transition metals in basic solvents such as pyridine and imidazole pioneered by Rauchfuss (eq 4).[24]

$$M + S_8 + 6Im \rightarrow [M(Im)_6]^{2+} + [S_8]^{2-} \quad (4)$$

The synthesis of **I** is a highly competitive reaction in which the formation of famatinite is minimized by the presence of excess iron. Not surprisingly, famatinite is only slightly more Cu rich/S poor, with respect to **I**. The fate of the extra iron metal could not be determined. However, no elemental iron was detected during Mössbauer investigations, thus leading us to conclude that it must still be in solution. Despite extensive variation of reaction conditions, we were never able to obtain **I** free of other impurities. Thus it is impossible to determine a quantitative yield, but it is clear that **I** is the overwhelming major product.

Under standard laboratory conditions, $[Fe(NH_3)_6]Cu_8Sb_3S_{13}$ is stable. A room-temperature X-ray powder diffraction pattern of **I** could be indexed with 37 reflections to a face-centered cubic unit cell with $a = 17.842(1)$ Å (Figure 1). The infrared spectrum of **I** showed absorption bands due to ammonia at 3370, 1635, and 1244 cm^{-1}, a broad band at 635 and 555 cm^{-1} due to δ(Fe−N−H), and bands at 365 and 283 cm^{-1} that most likely arise from M−S modes, where M = Cu or Sb.

Several unsuccessful attempts were made to remove some or all of the amines in **I** (vide supra) and create a microporous solid with catalytically active iron in the pores. The anionic framework of **I** resembles that of a zeolitic material (Figure 5); however, the free diameter of the pores that open into the iron hexaammine cavities are only about 1.5 Å across. Uncoordinated ammonia requires approximately a 3.1 Å diameter opening[25] to successfully diffuse through a crystalline framework without disrupting it.

Thermal analysis via DSC on **I** (which contained some residual Cu_3SbS_4 impurity) showed three strong but broad endotherms, centered at 230, 310, and 400 °C (Figure 6). XRD was utilized to characterize three samples that were taken through the first, second, and third endotherms, respectively (Figure 7). The first endotherm at 230 °C corresponds to the decomposition (probably via loss of ammonia) of **I**, which appears to form an X-ray amorphous material intermixed with the crystalline impurity Cu_3SbS_4. The XRD pattern of the sample after the second endotherm shows no further change and may be due to continued and complete loss of ammonia or a transition in Cu_3SbS_4. The XRD pattern of the sample after heating above the third endotherm shows the formation of iron-doped tetrahedrite, $Cu_{12-x}Fe_xSb_4S_{13}$. The composition of compound **I** is very similar to tetrahedrite, and thus it could be considered a precursor in which the necessary elements are mixed at the atomic level. This results in rapid formation of crystalline tetrahedrite at temperatures around 500 °C during DSC experiments.

Tetrahedrite is known to accommodate up to 16 wt % iron.[16] This cation substitution can be verified by analyzing the variation in the lattice parameters. Pure tetrahedrite crystallizes in a body-centered cubic unit cell with $a = 10.327$ Å[26] and the indexing of our mixed Fe/Cu tetrahedrite gave $a = 10.360(3)$ Å. This increase is consistent with the lattice parameters derived from naturally occurring tetrahedrite, which has been shown

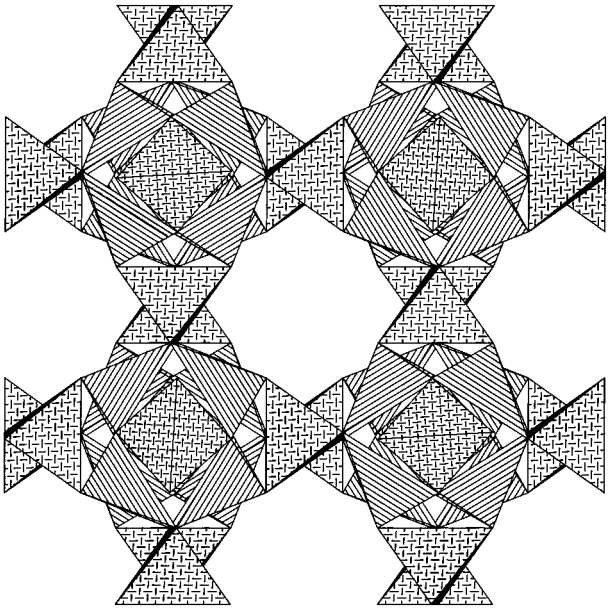

Figure 5. Polyhedral view of compound **I** with iron hexaammines omitted. Herringbone pattern are antimony-centered tetrahedra and copper-centered tetrahedra are striped.

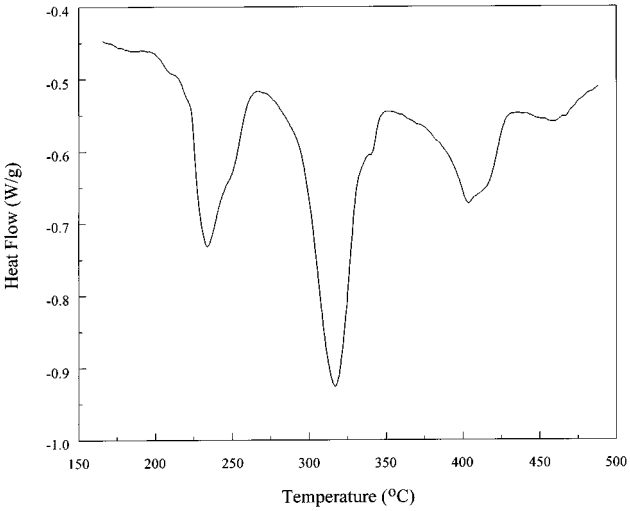

Figure 6. Differential scanning calorimetric thermogram for **I**. Decreasing values of heat flow are endothermic transitions.

(24) Dev, S.; Ramli, E.; Rauchfuss, T. B.; Wilson, S. R. *Inorg. Chem.* **1991**, *30*, 2514.
(25) See ref 20, p 476.
(26) JCPDS-ICDD database Joint Commission on Powder Diffraction Standards-International Center for Diffraction Data, Swarthmore, PA 19081.

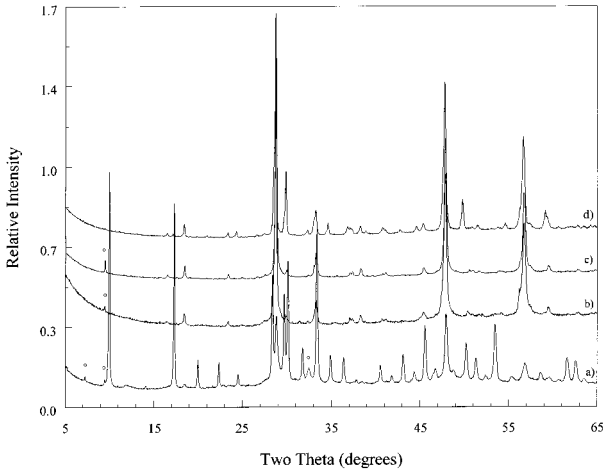

Figure 7. X-ray powder diffraction patterns for the stepwise decomposition of **I**, (a) as synthesized, (b) only famatinite after 265 °C, (c) only famatinite after 360 °C, and (d) tetrahedrite and famatinite after 500 °C. Denoted peaks: open circles are unknown.

to contain significant quantities of iron.[27] Studies on synthetically substituted tetrahedrite indicate that increasing iron content results in an increased lattice parameter.[28] On the basis of these studies, approximately 1.3 iron atoms are distributed over the 12 copper sites per formula unit. This value is in good agreement with the quantity of iron available from **I** (1.33 Fe/10.64 Cu).

A sample of **I** was also studied via TGA. The TGA trace shows only two plateaus, one at about 300 °C (about 17 wt % loss) and the other above 500 °C (about 23 wt % loss, total). Because the open diameter of the pores in $[Fe(NH_3)_6]Cu_8Sb_3S_{13}$ is only 1.5 Å, it was not expected that the loss of ammonia would occur easily or cleanly. At elevated temperatures, the flowing nitrogen atmosphere resulted in the deposition of sulfur at the cooler parts of the reaction vessel. The total loss of ammonia from the title phase accounts for only 7 wt %, so the simultaneous loss of sulfur must be occurring. The plateau at about 300 °C in the TGA thermogram may be a coincidental occurrence with respect to the 310 °C endotherm observed by DSC, and no connection between these phenomena can justifiably be made. The total weight loss observed would require loss of 50% of the sulfur in the title phase. The mass balance of the final product from the TGA could not be decisively made; XRD indicated that the products were tetrahedrite, Sb_2O_4 (probably formed from the presence of adventitious oxygen or water) and an unidentified phase with the characteristic $d = 9.288$ Å (vide infra). Surprisingly, there is no famatinite observed. The flow-through TGA system may be a factor in this outcome, since this conversion is observed at the same temperatures via DSC.

The substitution of copper with silver does not afford any compounds related to **I**. In fact, the incorporation of silver into iron hexaammine phases is not favorable and only a few yellow crystals of **II** were produced from the reaction conditions reported. Attempts to improve the yield have been unsuccessful. Although reproducibly prepared as a microcrystalline yellow powder, **III** decomposes to a black powder within minutes of exposure to the atmosphere, yielding a weakly diffracting mixture of Ag_2S, FeS, and potentially several unknowns. This behavior starkly contrasts that of alkali metal−silver−antimony sulfides.[3] Thus any further characterization has not been feasible. Likewise, the decomposition of **III** during X-ray data collection would seem to indicate that physical property measurements would result in limited valid data. The transparent, yellow color of **II** and **III** implies that they are electron-precise wide-bandgap semiconductors or insulators.

However, several other transition metals have been successfully substituted for iron and incorporated as amine-ligated metals in the structure type reported for **I**. Reaction conditions utilized in the synthesis of **I** also work equally well in the formation of microcrystalline black powders of $[M(NH_3)_x]Cu_8Sb_3S_{13}$ when $MnCO_3$ or Ni metal are used in place of iron. Again, famatinite is present and cannot be completely eliminated. For the Mn derivative, indexing of 38 reflections from X-ray powder diffraction data gave a face-centered cubic unit cell with $a = 17.875(1)$ Å. XRD indexing on the Ni substituted phase with 44 reflections gave $a = 17.736(2)$ Å, again with famatinite present (Figure 1).

Microcrystalline $[Mn(NH_3)_x]Cu_8Sb_3S_{13}$ was also studied by DSC. Two significant endothermic transitions occur over the temperature range examined, centered at 215 and 365 °C, with shoulders at 254 and 382 °C, respectively. Another endotherm at 316 °C was linked to the impurity Cu_3SbS_4. Again, XRD was utilized to study the resultant powders after intermediate heating cycles. After heating at 275 °C, a powder diffraction pattern of the sample was matched to Cu_3SbS_4, some tetrahedrite and an unknown phase with a similar d spacing ($d = 9.303$ Å) to that observed for the Fe analogue. The XRD pattern obtained from the DSC sample which had been heated to 500 °C showed more tetrahedrite, famatinite, and the same unknown phase observed from the 275 °C heating cycle ($d = 9.308$ Å). The substitution of Mn into the tetrahedrite structure type has been systematically studied and reported.[28] The lattice parameters derived from the Mn-substituted tetrahedrite formed during the DSC run gave $a = 10.430(2)$ Å, which implies about 2 Cu cations/formula unit are replaced by Mn cations.[28]

In contrast to the Fe and Mn cubic hexaammines, the DSC trace for $[Ni(NH_3)_x]Cu_8Sb_3S_{13}$ had one sharp endotherm at 230 °C and weak, broad endotherms at 306, 337, 446, and 469 °C. The XRD pattern of a sample that was heated at 250 °C indicated the presence of famatinite and tetrahedrite. Surprisingly, only tetrahedrite was present in the XRD pattern of the material subjected to the 500 °C heating. Nickel substitution in tetrahedrite has been observed previously.[16,28] Because lattice parameter changes are insensitive to substitution of Ni into this structure type, our $a = 10.324(1)$ Å is within the expected range but does not give any information on the quantity of substitution.[28] The cause of the weak endotherms in the DSC spectrum is unknown.

One common characteristic in the cubic hexaammines and their decomposition products was a peak with a d spacing of about 9.3 Å. This peak was found in the

(27) Peterson, R. C.; Miller, I. *Mineral. Magn.* **1986**, *50*, 717.
(28) Makovicky, E.; Karup-Møller, S. *N. Jb. Miner. Abh.* **1994**, 1, 89 and references therein.

Table 4. Bond Valence Sums

	$[Fe(NH_3)_6]Cu_8Sb_3S_{13}$	$[Fe(NH_3)_6]AgSbS_4$	$[Fe(NH_3)_6]AgAsS_4$
pnictide	4.77(9)	4.96(1)	5.16(7)
coinage metal	1.06(5) for Cu1 2.15(12) for Cu2	0.934(3)	0.95(1)
sulfur	2.16(7) for S1 1.23(5) for S2	1.475(4)	1.52(2)
iron	1.97(2)	1.94(3)	1.88(7)

initial reaction products for either Fe, Mn, or Ni. However, for manganese, it appeared to become more prominent during the decomposition studies, while it disappeared in the Ni case. For the Fe phase, it disappeared during DSC studies but became more pronounced during TGA investigations. Neither direct synthesis nor isolation of this impurity phase was possible, but it is likely that some phase between structure type **I** and tetrahedrite is formed.

The cations (Fe, Mn, Ni) utilized to form the cubic structure type **I** are not conducive to oxidation state determination, since all have multiple oxidation states available. If one assumes pentavalent antimony, monovalent copper, and divalent sulfur, then the hexaammine cation formally requires a trivalent charge. This assignment is contrary to the oxidation states observed in the many transition-metal hexaammine systems, such as compounds reported by Jacobs et al.,[19] the iron in **II** and **III**, and Mn(II) observed in four hexaammine compounds also prepared in this laboratory.[6] The lattice parameters derived for the three cubic phases provide no further insight.

An assessment of the oxidation states present in **I**−**III** was undertaken using bond valence sum methods reported by Brown and Altermatt.[29] Bond valence sum calculations are an empirical method for determining the oxidation state of atoms. The calculation is based strictly on bond distances and some predetermined single bond distance for a M−L bond. The sum of all the individual M−L bond strengths around M results in the oxidation state of M. Table 4 lists the results of these calculations. For **II** and **III**, the oxidation states of iron, silver, and pnictide atoms are unambiguous (+2, +1, and +5, respectively) and result in charge-balanced systems. This is consistent with their transparent yellow color. The low oxidation states calculated for the sulfur atoms in these two systems are probably the result of their rather low coordination number to metal atoms and their potential for hydrogen bonding, which was not included in these calculations.

Unfortunately, the situation is not as straightforward for compound **I**. The oxidation state of the crystallographically unique antimony atom is clearly +5, which is in accord with its tetrahedral coordination. However, these calculations are not so decisive for any of the other atoms. The S1 atom appears to have a typical −2 valence, while that calculated for the S2 atom is low. This may be explained by the very unusual coordination environment of S2 and its long distances to metal atoms (vide supra). Given that the overwhelming majority of Cu atoms are monovalent in copper-containing sulfosalts, it would make sense to assign the cluster anion as $[Cu_8Sb_3S_{13}]^{3-}$ with each copper atom formally Cu(I), the antimony atoms as Sb(V), and the sulfur atoms as divalent sulfides. This would formally assign the countercation as $[Fe(NH_3)_6]^{3+}$, which is quite reasonable. However, a closer examination reveals several problems with this interpretation. There is only one unique iron site, and its bond valence sum was determined to be +2. Given the large experimental uncertainty in iron hexaammine bond distances, this is not so troubling. However, there are two unique copper sites, and a careful examination of the Cu valence sums indicates that one site is best assigned as Cu(I) and the other as Cu(II). The bond distances utilized in this calculation are much more reliable and would result in the iron formally being Fe(−I). This is obviously not a useful interpretation, but the apparent low valence of the iron site, and the greater than normal valence of one of the copper sites, along with the observation that the normally divalent metals manganese and nickel can readily substitute for iron, all suggest very strongly that both metals (Fe and Cu) are present with mixed valency. This is not unusual in many sulfosalt derivatives. For example, tetrahedrite, $Cu_{12}Sb_4S_{13}$, readily incorporates iron and other metals into copper sites and has a complex mixed valent electronic structure.[16,28]

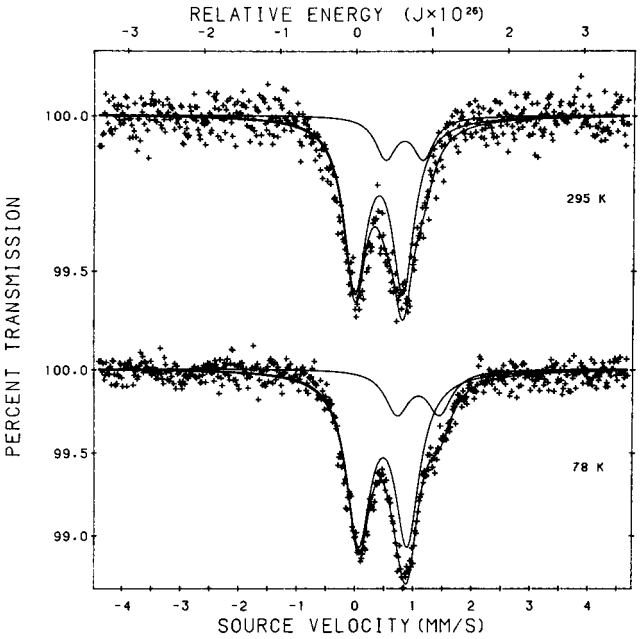

Figure 8. Mössbauer spectra for **I** at 295 K (top) and 78 K (bottom).

In an attempt to gain further insight into the valence states of the iron centers, Mössbauer spectroscopy was performed on compound **I** at 295 and 78 K (Figure 8). These results indicate that Fe(II) is present in approximately 20% abundance assuming equivalent recoil-free fractions. Since this assumption is not completely valid and the recoil-free fraction for Fe(II) is generally lower than Fe(III), the 20% value represents a lower limit of Fe(II) content. Spectral parameters are given in Table 5.

(29) Brown, I. D.; Altermatt, D. *Acta Crystallogr.* **1985**, *B41*, 244.

Table 5. Mössbauer Spectral Hyperfine Parameters for $[Fe(NH_3)_6]Cu_8Sb_3S_{13}$

temp (K)	δ[a] (mm/s)	ΔE_Q (mm/s)	Γ (mm/s)	area (%)	assignment
295	0.40	0.82	0.46	81	high-spin Fe(III)
	0.93	0.65	0.44	19	high-spin Fe(II)
78	0.48	0.83	0.51	80	high-spin Fe(III)
	1.09	0.73	0.50	20	high-spin Fe(II)

[a] Relative to room-temperature natural α-iron foil.

All the δ and ΔE_Q values and their change with temperature are reasonable. The isomer shifts are very typical of iron(II) and iron(III) in an ammine environment. It should be noted that the quadrupole splittings, ΔE_Q, are smaller than is usually observed for iron(II) complexes. This occurs because the iron(II) ion is in a nearly cubic local environment and as a consequence, the valence contribution to the electric field gradient, EFG, is virtually zero. Thus the observed quadrupole splitting must result from a lattice contribution to the EFG. This also accounts for why the quadrupole splittings are so similar for the iron(II) and iron(III) sites. For the iron(III) site, with an $^6A_{1g}$ ground state, there is of course no valence contribution to the EFG, and only a lattice contribution is observed. Thus, because the splitting in the iron(II) complexes is slightly smaller than for the iron(III) complexes, the small valence contribution for iron(II) must subtract from the lattice contribution. Although limited by data at only two temperatures, $d\delta/dT$ appears to indicate that the covalency of Fe(III) to six ammonias is about twice that for Fe(II), this is not unreasonable. The most unusual feature is the line width, Γ, which is about twice as large as one might expect. This may very well be reasonable for iron weakly bound to six ammonia ligands.

These results indicate that the formal valencies of iron and copper in compound **I** are probably mixed. Ideally, an equal mixture of Fe(II) and Fe(III) would lead to a valence-precise, closed-shell arrangement if all Cu1 were monovalent and all Cu2 were divalent, as suggested by the bond valence calculations and observed bond lengths. However, the Mössbauer data suggest that the ratio of Fe(II)/Fe(III) is not 1:1. It is important to note that copper chalcogenides are uniquely complex systems, and assigning formal valence states is difficult in even the seemingly simplest cases. For example, the apparently straightforward CuS is actually a mixture of Cu(I), S_2^{2-}, and S^{2-}[30]. In most cases, the copper centers are really Cu(I) with the Fermi level in a band consisting of mostly chalcogenide p orbitals. Thus in a complex system such as **I**, it is likely that not only are there mixed valent iron centers, but there are probably mixed Cu(I)/Cu(II) centers as well as delocalized holes among the antimony sulfide framework.

Acknowledgment. We are indebted to the National Science Foundation for support of this work (CHE-9102548) and the diffractometer (CHE-9207230). We are grateful to Shiou-Jyh Hwu and Richard A. Mackay for use and assistance of the TGA apparatus and Mr. D. Vandormael for obtaining the Mössbauer spectra.

Supporting Information Available: Anisotropic thermal parameters and discussion, hydrogen atom positional parameters and bonding considerations, complete crystallographic details, derived lattice parameters, impurity *d* spacings for compounds with structure type **I**. Also included are full thermal ellipsoid plots, DSC and TGA spectra, and X-ray diffraction patterns from the decomposition studies of $[M(NH_3)_x]Cu_8Sb_3S_{13}$ (25 pages); structure factor tables (7 pages). Ordering information is given on any current masthead page.

CM970095C

(30) (a) Flomer, J. C. W.; Jellinek, F. *J. Less-Common Met.* **1980**, *76*, 153. (b) Viola, F.; Schöllhorn, R. *J. Chem. Soc., Chem. Commun.* **1982**, 907.